




Study the effect of space radiation on ISO-type multijunction solar cells

B. R. Uma^{1,*} , Sheeja Krishnan², V. Radhakrishna¹, and M. Sankaran¹

¹U.R.Rao Satellite Center, Bengaluru, India

²ShreeDevi Institute of Technology, Kenjar, Mangaluru, India

Received: 27 November 2020

Accepted: 15 April 2021

Published online:
6 May 2021

© The Author(s), under exclusive licence to Springer Science+Business Media, LLC, part of Springer Nature 2021

ABSTRACT

Multijunction, GaInP/GaAs/Ge tandem solar cells have been extensively used in space as the power generation source for satellites due to their high conversion efficiency, high radiation tolerance and low-temperature coefficient. The most critical characteristic of space solar cells is the radiation hardness of the device. The space radiation environment degrades the long-term performance of the solar cell when they are exposed to the radiation. The effect of radiation on single-junction cell is well understood, established and well-studied. But the radiation effect on multijunction solar cell and its characterization needs to be studied in detail. The study is carried out on the effect of space radiation on ISO-type (sub-cells) cells of multijunction solar cells, its characterization and compared with the full cell and among three sub-cells which one is more susceptible to radiation. Different characterization techniques Dark IV, Light IV, Spectral Response and Electroluminescence are used to characterize sub-cells as well as full cell. The reverse saturation current, solar cell ideality factor, electrical parameters, current density, series and shunt resistance of sub-cells and full cells were estimated for pre and post-electron and proton radiation. This study helps in optimization of the solar cell design, material selection and manufacturing processes of multijunction solar cell. Also, the results of this study are useful in modeling of multijunction solar cell.

1 Introduction

Photovoltaic Solar cells are the main power generation source for satellites because of their low cost, robustness and reliability. Single-junction solar cells are generally made with single P–N junction and single material, the efficiency of commercially available GaAs based single-junction is ~ 18.5% and

utilizes sun spectrum up to 900 nm wavelength [1]. Due to improvement in the solar cell technology, the state-of-the-art multijunction solar cells with conversion efficiency 30% are available for powering the spacecraft [2, 3].

Multijunction solar cells more specifically triple junction solar cells are formed or constructed by monolithically connected three solar cells and two

Address correspondence to E-mail: umabr21@gmail.com

tunnel diodes to utilize the full sun spectrum [1, 2], which in turn improves the efficiency of solar cell and specific power (W/m^2) [1, 2] of solar array. In recent times, solar cell researchers/manufacturers use lattice matched four to five solar cells for the construction of multijunction solar cells, but four and five junction solar cells are still in the development stage and not qualified for the space use. At present only three junction solar cells are extensively used in space industry for powering the spacecraft. Hence, in this study we have taken the three junction solar cells.

Space radiation consists mainly of energetic protons and electron particles [3] of different energies. Many studies have shown that the middle GaAs solar cell is more susceptible to the radiation environment [2, 3]. The middle cell degrades more with radiation compared to the top sub-cell. The impact of the low voltage and high current density bottom Ge sub-cell's effect on the overall performance of the triple junction cell is insignificant. Once the intermediate GaAs sub-cell is significantly damaged by irradiation, photovoltaic parameters of full cell are affected. The impact of radiation on different sub-cells is not similar; therefore, it is necessary to perform a separate radiation damage study on the sub-cells of the multijunction solar cell to understand the mechanism [4]. This study will help in the optimization of the solar cell design and manufacturing processes [4]. Also helps in understanding the performance of solar cell for the spacecraft mission life and predict the power output from the solar cells in the space.

Space radiation contains mainly energetic proton, energetic electrons, gamma rays, Galactic gamma rays (GCR), and X-rays. Due to the earth's magnetic field, the charged particles are trapped. Among these species, the trapped electron and trapped proton affect the solar cells significantly, as they create displacement damage in the solar cells. The displacement of the atoms creates defects in the solar cell crystal lattice and these defects act as recombination centers and reduces the electrical performance of the solar cell [4]. The near-earth space radiation where our satellites orbits, contains protons and electrons of different energies. The electron energy ranges from hundreds of keV (kilo electron Volt) to 7 MeV (Mega electron Volt), and the proton energy ranges from a few 100KeV to a few hundred MeV (solar flare proton). The solar cell damage equivalence of the various energy electrons and protons for total mission life is normally expressed in terms of damage equivalent by

1 MeV electrons and 10 meV protons. Many studies have been carried out on these multijunction solar cells for electron and proton radiation of different energies. In the present study emphasis put on 1 MeV electron and 10 MeV proton radiation, since it is very important for space application.

In this paper, the studies are carried out on the effect of 1 MeV electron and 10 MeV proton radiation on the multijunction cell as a full cell as well as on sub-cells/ISO-type cells. The ISO-type solar cell samples were irradiated with proton and electron radiation of different fluence in India. The samples were characterized before and after irradiation for electrical performance and device characterization using different techniques like light and dark IV measurements, Spectral response, electroluminescence, and the results are presented and discussed in this paper.

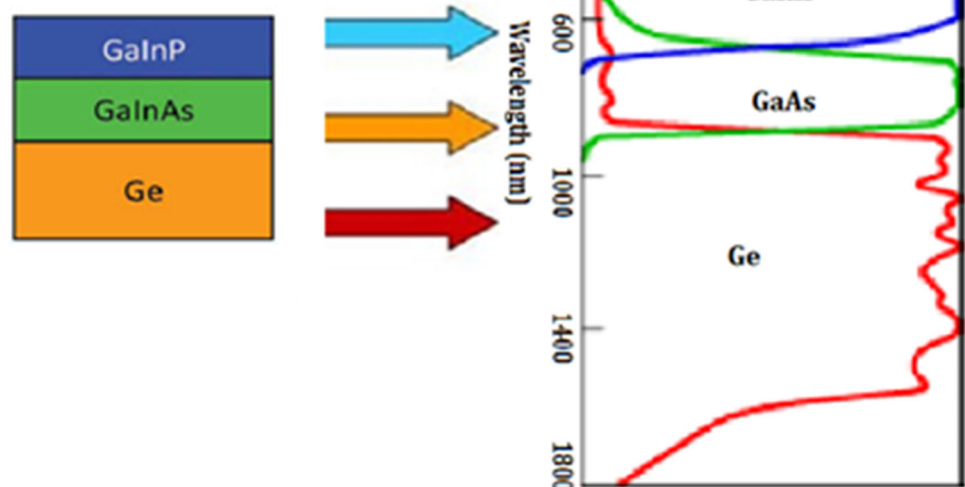
2 Multijunction solar cells

Multijunction solar cells used for power generation in space consist of GaInP top junction with bandgap energy of 1.7–1.9 eV, GaAs middle junction with 1.3–1.4 eV, and a Ge bottom junction with 0.7 eV. A typical multijunction solar cell structure is shown in Fig. 1 and the response of each sub-cell to the solar spectrum (typical) is shown in Fig. 2. Single-junction solar cells like silicon and GaAs/Ge utilize solar spectrum up to 1100 nm. The single-junction solar cell can generate higher current due to photon absorption over the broader spectral region but cannot produce high open circuit voltage due to limitation in the dark current of the low bandgap material. Also, single-junction solar cells cannot split the solar spectrum more effectively because of bandgap limitations and lower optical sensitivity and lower absorption. To overcome these drawbacks, the multijunction solar cells are formed with many sub-cells of different energy gap materials and effectively split the solar spectrum and utilizes the full solar spectrum. The usage of three different bandgap materials generates more open circuit voltage. Due to these improvements, the efficiency of multijunction cells is around 30%, which is more than any space-grade single-junction solar cell $\sim 18.5\%$ (achieved efficiency). This improved efficiency will reduce the area and weight of the spacecraft solar panels and



Fig. 1 Typical multijunction solar cell structure

Fig. 2 Spectral utilization in multijunction solar cells



increases the specific power W/m^2 capacity of solar panels, helps in reducing the Launch cost.

Sub-cells of multijunction solar cells are generally called ISO-type cells. ISO-type solar cells are fabricated such that only one of the three P–N junctions in the multijunction solar cell is active electrically and the other two junction's photon absorption characteristics and the electrical behavior of the tunnel diodes are simulated [2, 25]. All characterization of the ISO-type solar cells in this study is carried out with the assumption that the only the particular sub-cell is active and rest of the sub-cells does not impact the measured performance of the active P–N junction in them.

The four ISO-type cells are composed as follows:

- Triple junction (TJ) full cell: InGaP/InGaAs/Ge.
- Top Cell: InGaP/Ge with InGaP active cell.
- Middle Cell: GaAs/Ge with GaAs active cell.
- Bottom cell: Ge cell.

3 Experimental methods

Since the impact of particulate radiation on the performance of the multijunction solar cell is affected by the behavior of each of the junctions, it is, therefore,

necessary to perform separate radiation damage studies on each of the sub-cells. Illuminated current–voltage (I – V) characteristics, spectral response (SR)/quantum efficiency, and electroluminescence were performed pre- and post-irradiation to evaluate the impact of irradiation.

Illuminated IV characteristics were performed under 1AM0 X-25 solar simulator with a temperature-controlled mount. The measurement is carried out at 28 °C for pre- and post-radiation comparison purposes, the results can be extrapolated to any temperature using temperature coefficients. Generally, the space-grade solar cells will be characterized at Air Mass Zero (AM0) to simulate space conditions. Where 1AM0 is the intensity and spectrum above the earth’s atmosphere. The simulator was calibrated using a secondary standard solar cell set which is calibrated using primary standard by balloon flight. The spectral response was measured using a monochromator that was calibrated using a silicon photodiode and InGaAs diode. Electroluminescence spectrum of ISO-type cells are measured, using 25 mw Argon (Ar) laser. The solar cells were irradiated with 1 meV electron and 10 meV proton for different fluences at Electron Beam Center (EBC) and Tata Institute of fundamental research (TIFR), Mumbai, India.

4 Results and discussion

4.1 Reverse saturation current and diode ideality factor

4.1.1 Method I

The saturation current (I_0) and ideality factor (n) of a P–N junction solar cell are an indication of the quality of the cell. These two parameters are usually estimated from dark I – V measurement.

The solar cell equivalent circuit model can be represented by a circuit shown in Fig. 3. This solar cell model has been used widely for solar cell analysis with some minor deviations [5–7] for dark IV.

Based on the equivalent circuit of a photovoltaic solar cell, the characteristic equation that gives the relationship between the terminal voltage and the current generated can be written as follows [5, 6]:

For Dark IV, the equation can be written as (7)

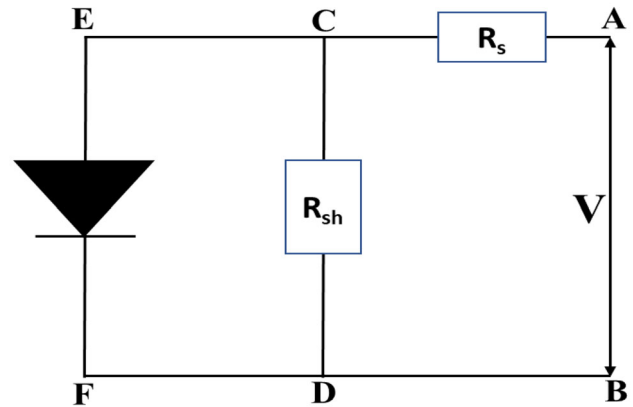


Fig. 3 Solar cell equivalent circuit

$$I_D = I_0 \exp\left(\frac{qV}{nkT} - 1\right) \tag{1}$$

where I_D Dark current (A), I_0 reverse bias saturation current (A), V cell voltage (V), q electron charge 1.6×10^{-19} (C), n ideality factor, K Boltzmann’s constant 1.38×10^{-23} (j K^{-1}), T absolute temperature of the junction.

The ideality factor which is a measure of how closely the diode follows the ideal diode equation is derived from the slope of the dark IV characteristics and it varies from 1 to 5.

For $V > 50$ mV, the term (-1) can be ignored and the Eq. 1 can be rewritten as

$$I = I_0 \exp\left(\frac{qV}{nkT}\right) \tag{2}$$

Equation 2 is written as [7]

$$\ln(I) = \ln(I_0) + \left(\frac{q}{nkT}\right)V \tag{3}$$

$$n = \frac{grad}{kT/q}$$

$$\ln(I_0) = \frac{-y}{nkT/q}$$

Plotting the natural log of the current against the voltage, the slope q/nkT gives n and the intercept gives $\ln(I_0)$ [7].

The dark IV characteristics of ISO-type solar cell is measured pre- and post-irradiation. The observed change is an increase in the dark current at any given voltage for each cell after radiation and is inferred as due to the introduction of defects after irradiation. The ideality factor and reverse saturation current of

Fig. 4 Dark IV plots of samples pre and post-radiation

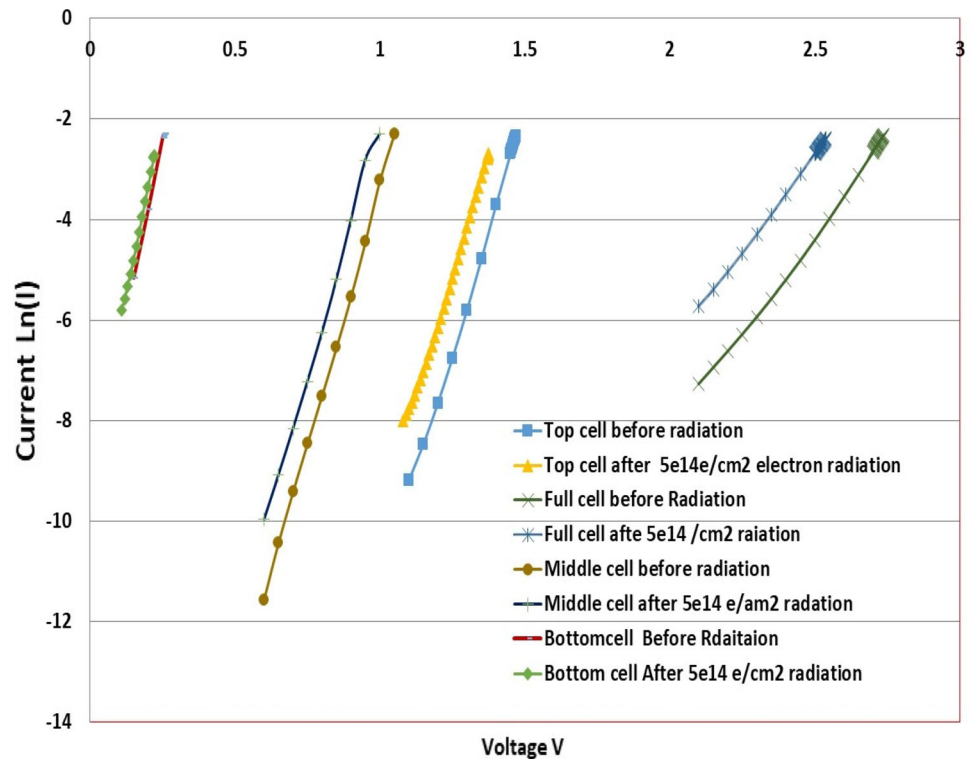


Table 1 I_0 and n values measured by Method I

Electron Radiation Dose	Initial		1E14e/cm ²		5E14e/cm ²	
	Reverse saturation current I_0 (A)	Ideality Factor n	Reverse saturation current I_0 (A)	Ideality Factor n	Reverse saturation current I_0 (A)	Ideality Factor n
Top (GaInP)	4.5×10^{-14}	2.15	2.0×10^{-13}	2.06	3.9×10^{-13}	1.99
Middle (GaAs)	6.0×10^{-12}	2.00	4.5×10^{-11}	1.93	2.7×10^{-10}	1.88
Bottom (Ge)	4.5×10^{-05}	1.41	1.4×10^{-04}	1.36	1.5×10^{-04}	1.26
Full cell	4.5×10^{-11}	4.85	7.5×10^{-11}	4.77	1.1×10^{-10}	4.22
By adding All Iso-type Solar cells (full cell)	5.0×10^{-11}	5.56	2.48×10^{-10}	5.35	5.42×10^{-10}	5.13

each sub-cell are estimated from the dark IV characteristics by Eq. 3 and plotted as shown in Fig. 4.

The saturation current and diode ideality factor for full cell and sub-cell of multijunction cells are measured and listed in Tables 1 for pre- and post-electron radiation test.

In dark I - V , voltage (V) is applied across A and B.

Two cases can be discussed as follows:

Case 1: At Low voltages, i.e., at $V < V_{knee}$ (V_{knee} = External biasing voltage at which current increases rapidly).

In this case, diode will not conduct and current will pass through the shunt resistance (C to D). Current (I) will be calculated as

$$I = \frac{V}{R_{sh} + R_s}$$

It can be seen that, in this case $R_{sh}/R_s \gg 1$. Thus $R_{sh} + R_s \approx R_{sh}$, so the contribution of R_s in controlling the current is negligible. At low voltages, the ideality factor is governed by the shunt paths across the P-N junction.

As I_0 and n are calculated by fitting the semi log plot of log (current) vs. voltage below (at low voltage) the V_{knee} , thus R_s will not play any role.

Case 2: At High voltage, i.e., at $V > V_{knee}$.

Above V_{knee} , the diode will start to conduct (current path is EF) and R_s will be deciding factor of the current in the circuit. The effect of series resistance on $I-V$ will be described as the decrease of slope of the IV with the increase of R_s above V_{knee} and the ideality is governed by R_s at higher voltages.

The ideality factor reduces with radiation exposure, this indicates that the radiation exposure creates defects due to displacement damage and increases the radiative recombination in the solar cells. But the saturation current increases with radiation, which indicates the decreased diffusion length and reduced minority carrier lifetime after radiation.

The decrease in the ideality factor of all three sub-cells GaInP, GaAs and Ge junction decreases the open circuit voltage (V_{oc}) as shown in Eq. 4 and maximum power due to irradiation. Also, the voltages of all sub-cells reduce with the radiation.

$$V_{oc} = \frac{nkT}{q} \ln\left(\frac{I_L}{I_0} + 1\right) \tag{4}$$

where I_L light-generated current, I_0 diode saturation current, n Ideality factor, q electronic charge 1.6×10^{-19} (C), V_{oc} Cell open circuit voltage, K Boltzmann’s constant 1.38×10^{-23} (j K⁻¹), T Absolute temperature in kelvin.

Dark $I-V$ measurements suggest that the radiation primarily affects dark current produced at voltages greater than 0.5 V. The dark saturation current of irradiated solar cells increases but simultaneously decreases the ideality factor due to reduction in the open circuit voltage [8–10]. Also, a reduced ideality factor further indicates a change in the radiative

recombination mechanism and increase in the recombination current in the solar cells after exposure to radiation.

4.1.2 Method II

In this method, the ideality factor and reverse saturation current is estimated using Eqs. 5 and 6 [11] with parameters generated from light IV. The parameters R_s , R_{sh} , I_{mp} , V_{mp} , V_{oc} and I_{sc} of sub-cells and full cells are taken from Tables 3 and 4. The estimated reverse saturation current I_0 and ideality factor n is listed in Table 2. The results of method II from light IV are listed in Table 2. In both methods the ideality factor decreases with radiation and saturation current increases with radiation and this is due to radiation-induced defects.

$$n = \frac{V_{mp} + I_{mp}R_s - V_{oc}}{V_t \left[\ln\left(I_{sc} - \frac{V_{mp}}{R_{sh}} - I_{mp}\right) - \ln\left(I_{sc} - \frac{V_{oc}}{R_{sh}}\right) + \frac{I_{mp}}{I_{sc} - \frac{V_{oc}}{R_{sh}}}\right]} \tag{5}$$

$$I_0 = \left(I_{sc} - \frac{V_{oc}}{R_{sh}}\right) \exp\left(\frac{-V_{oc}}{nVt}\right) \tag{6}$$

where V_{oc} : the open circuit voltage, I_{sc} : the short circuit current, V_{mp} : Voltage at Maximum power point, I_{mp} : Current at Maximum power point, R_s : Series Resistance, R_{sh} : Shunt Resistance, n : Ideality Factor, Vt = Thermal Voltage 26 mV.

4.2 Estimation of series and shunt resistance

The solar cell Eq. 7 under practical test conditions can be written with series and shunt resistance as [5, 6]

$$I = I_L - I_0 \left[\exp\left(\frac{q(V + IR_s)}{nkT}\right) \right] - \frac{V + IR_s}{R_{sh}} \tag{7}$$

Table 2 I_0 and n values estimated using Method II

Electron Radiation	Initial		After 1E14 e/cm ²		After 5E14 e/cm ²	
	Reverse saturation Current I_0 (A)	Ideality Factor n	Reverse saturation Current I_0 (A)	Ideality Factor n	Reverse saturation Current I_0 (A)	Ideality Factor n
Top (GaInP)	1.66×10^{-21}	1.44	5.19×10^{-19}	1.34	1.59×10^{-18}	1.16
Middle (GaAs)	2.24×10^{-16}	1.51	1.2×10^{-15}	1.2	4.91×10^{-13}	1.07
Bottom (Ge)	5.74×10^{-7}	1.195	6.64×10^{-5}	1.193	5.4×10^{-5}	0.717
Full cell	6.08×10^{-20}	2.94	4.53×10^{-19}	2.5	9.99×10^{-17}	2.45

Table 3 Pre- & Post-Irradiation Measurements of R_s & R_{sh}

Resistance in Ohm	Before Radiation test	After Radiation test	Before Radiation test	After Radiation test
	R_{sh}	R_{sh}	R_s	R_s
Full Cell				
Sample 1	1576	1480	1.500	2.520
Sample 2	1575	1508	1.480	1.519
Sample 3	1576	1467	1.470	1.586
Sample 4	1575	1463	1.419	1.600
Top Cell				
Sample 1	841	805	0.740	0.909
Sample 2	837	264	0.769	0.901
Sample 3	837	387	0.838	0.937
Sample 4	837	818	0.750	0.958
Middle Cell				
Sample 1	83	37	0.375	0.586
Sample 2	84	40	0.411	0.632
Sample 3	98	66	0.571	0.672
Sample 4	84	65	0.571	0.714
Bottom Cell				
Sample 1	74	28	0.225	0.294
Sample 2	74	36	0.25	0.303
Sample 3	76	48	0.246	0.281
Sample 4	74	50	0.218	0.245

[Sample 1 and 2 are irradiated for 1 MeV electron, $5E14e/cm^2$, $1E14e/cm^2$ fluence, respectively, sample 2 and 3 are irradiated for 10 MeV Proton of $1E12 p/cm^2$, $5E12p/cm^2$, respectively.]

where R_s series resistance, R_{sh} shunt resistance, I Solar cell output current, I_L light-generated current, I_0 diode saturation current, n Ideality factor, q electronic charge 1.6×10^{-19} (C), V cell's terminal voltage, K Boltzmann's constant 1.38×10^{-23} (j K⁻¹), T Absolute temperature in kelvin.

This equation has been used widely for solar cell analysis with minor deviations. The reason for deviation is due to difficulty in measuring the series and shunt resistance.

R_s and R_{sh} are the effective internal resistances in series and in shunt to the cell associated. The series resistance R_s is due to the sheet resistance of the semiconductor material, the metal contacts and interconnects and contact resistances between the semiconductor and the metal contacts. The shunt resistance. R_{sh} is due to non-idealities, manufacturing/growth defects and impurities in the P–N junction [12].

In this method, a linear fitting of IV curve region near open circuit voltage (V_{oc}) is used for series resistance estimation and short circuit current (I_{sc}) region for shunt resistance estimation of a solar cell.

The slopes at V_{oc} and I_{sc} region give a good approximation for R_s and R_{sh} and provide a good indication of defects introduced by radiation, operating temperature, etc.

The series and shunt resistances were estimated from AM0 illuminated I – V characteristics and listed in Table 3, R_{sh} values changes after radiation. Shunt resistance decreases with the radiation and as well as with increased fluence due to manufacturing defects and structural damage which acts as recombination centers induced by radiation [13]. The increased series resistance due to radiation reduces fill factor of solar cell.

4.3 Electrical performances under AM0

Radiation creates displacement damage and results in defects in the solar cells. The defects induced by radiation causes a reduction in the minority carrier lifetime. This results in a reduction in the I – V performances of the solar cells under AM0 spectrum. The reduction depends on the type of radiation, on its energy, and the total fluence [12, 14, 15].

The electrical parameters of I_{sc} —short circuit current, V_{oc} —open circuit voltage V_{mp} —Voltage at the maximum power point, I_{mp} —current at maximum power point, conversion efficiency η and fill factor after irradiation with 1 MeV electrons and 10 MeV proton having different fluences of sub-cells and full cell are listed in Table 4. The light IV (Current Voltage) characteristics of bottom cell, middle cell, top cell and full cell is shown in Fig. 5.

The conversion efficiency and fill factor (FF) of all the sub-cells is affected by radiation. The pre and post-radiation electrical parameters I_{sc} , V_{oc} , V_{mp} , I_{mp} , efficiency and FF are shown in Table 4. The FF and conversion efficiency are represented by below equations. Both Voltage and current values decrease with radiation exposure and resulted in change in FF and conversion efficiency.

The FF and efficiency are calculated from Eq. 8 and 9.

$$FF = \frac{V_{mp}I_{mp}}{V_{oc}I_{sc}} \tag{8}$$

$$\eta = \frac{V_{mp}I_{mp}}{P_{in}} \tag{9}$$

where V_{oc} : the open circuit voltage, I_{sc} : the short circuit current, V_{mp} : Voltage at Maximum power point, I_{mp} : Current at Maximum power point, P_{in} is input power, FF is the fill factor and η is the efficiency.

From the electrical parameters listed in Table 4, it is clear that the radiation affects the performance of solar cell, which reduces the current and voltage of all sub-cells. More degradation happens at higher fluences. Also, the effect of proton is more compared to electron radiation.

The main interactions of concern when irradiating solar cells with electron and proton radiation are ionization and atomic displacement [16]. In solar cell, the major interaction is due to atomic displacement. Atomic displacement occurs when energetic particles interact with atomic structure and resulted in a displacement of an atom within the materials structure. A displaced atom within the crystal lattice will result in the formation of an interstitial defect atom, a vacancy, and other electronic and phonon losses. Displaced atoms will form stable defects and causes permanent degradation in the solar cell [17]. Due to this, energy levels are formed within the bandgap of the material and act as trapping centers. The traps between the valance band and conduction band are

distributed in the material due to radiation and act as recombination centers and alters the electrical performance of solar cell.

From the results it is clear that, the electrical parameters of both current and voltage of top GaInP is better and less degraded compared to middle GaAs solar cell and it indicates that the radiation-induced degradation is more in middle GaAs solar cell [8] compared to GaInP.

4.4 Spectral response and J_{sc} estimation

Spectral response (SR) is one of the major characterization techniques used to evaluate the solar cell damage caused by radiation. The spectral response curve represents the “conversion ability” of the solar cell as a function of the incident light wavelength. The changes in the SR curve are related to the degradation in the performances of the solar cell.

In particular to the degradation of the carrier lifetimes that implies a lower capacity of the P–N junction to collect the photogenerated photocarriers and it will be reflected in the current density of the solar cell. From the spectral response one can calculate the current density of the solar cell using the Eq. 10,

$$J_{sc} = \int_{\lambda_1}^{\lambda_2} S(\lambda)E(\lambda)d\lambda \tag{10}$$

where J_{sc} Current Density in $A\ m^{-2}$, λ Wavelength nm, $S(\lambda)$ Spectral response of the material $AW^{-1}nm^{-1}$, $E(\lambda)$ Energy of the solar spectrum $Wm^{-2}nm$.

The spectral response (SR) of top and middle junction solar cells is shown in Fig. 6 and SR of the bottom solar cell is shown in Fig. 7. The current density J_{sc} of ISO-type sub-cell and the full cell is estimated from the spectral response curve and listed in Table 5.

The change in the SR is related to the radiation-induced defects which reduces the diffusion length [6] of light-generated carriers and impact on the carrier collection efficiency and reduces the current generation [10, 18].

The SR of the top GaInP solar cell shows that there is little or no degradation at the lower wavelengths (300–400 nm), whereas around 550 nm there is a small degradation. The change in the SR is related to the defects induced by radiation, which reduces the diffusion length of the carriers and results in the reduction in the carrier collection efficiency and current.

Table 4 Pre- & Post-irradiation electrical parameters of sub-cells /ISO-type cells and full cell

Parameters	Initial	10 meV Proton		1 meV Electron	
		1E12 P/cm ²	5E12 P/Cm ²	1E14 e/cm ²	5E14 e/cm ²
Top Cell					
J_{sc} (mA/Cm ²)	17.5	17.25	17	17	17
J_{mp} (mA/cm ²)	16.75	16.25	16	16.3	16
V_{mp}	1.275	1.192	1.17	1.214	1.203
V_{oc} (V)	1.431	1.358	1.327	1.376	1.357
Efficiency (%)	15.784	14.31	13.83	15.05	14.46
Fill Factor (%)	85.28	82.68	82.98	84.59	83.43
Middle cell					
J_{sc} (mA/Cm ²)	19.5	19.25	19	18.75	18.75
J_{mp} (mA/cm ²)	18	17.25	16.75	17.5	17.15
V_{mp}	0.86	0.771	0.75	0.814	0.802
V_{oc} (V)	1.008	0.912	0.894	0.99	0.93
Efficiency (%)	11.44	9.8	9.28	10.52	10.22
Fill Factor (%)	78.75	75.75	73.95	76.74	78.49
Bottom Cell					
J_{sc} (mA/Cm ²)	52	45	43	51	45
J_{mp} (mA/cm ²)	44	38.25	36.75	42	38.75
V_{mp}	0.183	0.152	0.147	0.168	0.155
V_{oc} (V)	0.256	0.245	0.239	0.248	0.235
Efficiency (%)	5.95	4.3	3.4	5.21	4.45
Fill Factor (%)	60.4	52.73	52.56	55.78	56.79
Full cell					
J_{sc} (mA/Cm ²)	17.25	17	17	17.1	16.75
J_{mp} (mA/cm ²)	16.75	16.5	16.25	16.5	16.3
V_{mp}	2.413	2.21	2.189	2.32	2.2
V_{oc} (V)	2.705	2.539	2.512	2.612	2.514
Efficiency (%)	29.97	26.95	26.29	28.29	26.5
Fill Factor (%)	86.61	84.48	83.29	85.7	85.15

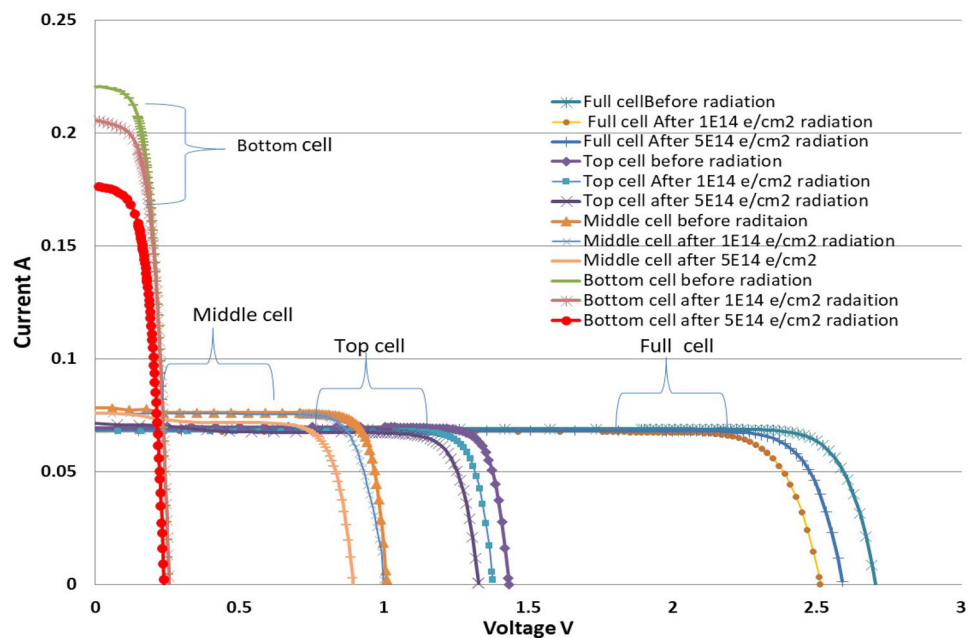
Fig. 5 Light IV characteristics of bottom cell, middle cell, top cell and full cell after 1 MeV electron radiation

Fig. 6 Top and middle Cell SR as a function of irradiation

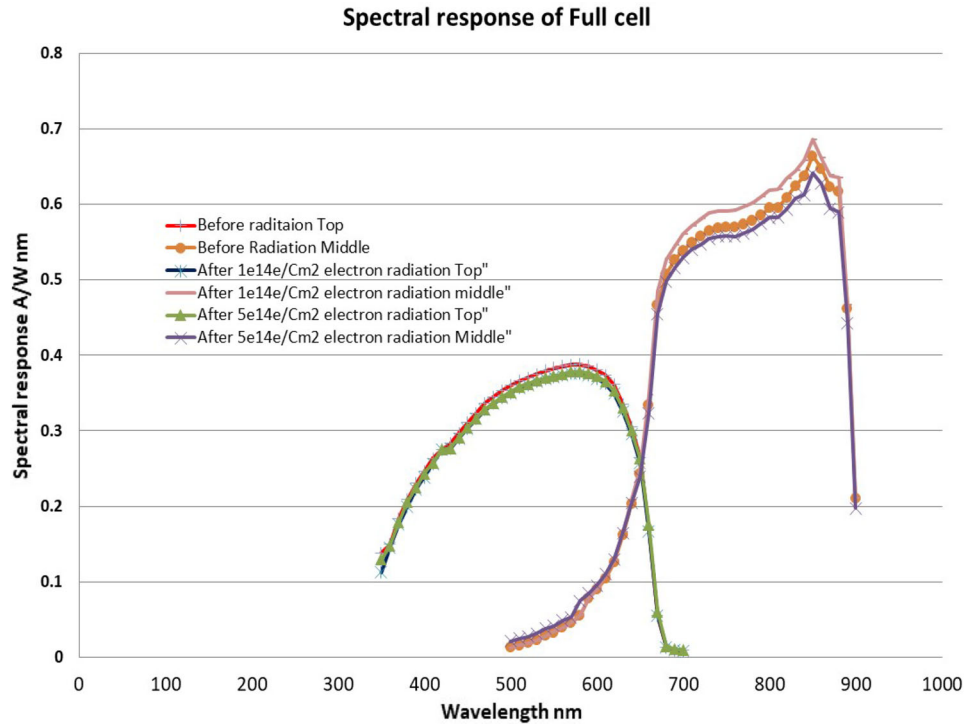
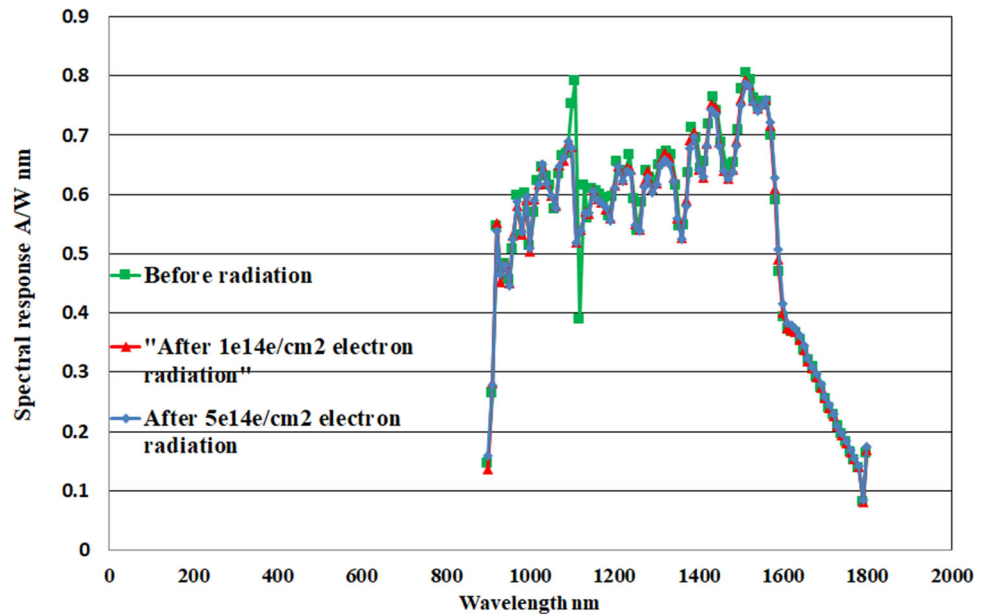


Fig. 7 Bottom cell SR as a function of irradiation



The degradation is more pronounced in the middle GaAs junction; this is consistent with the observation that, GaAs middle junction is more prone to radiation and degrades more [7].

The degradation in the SR of the bottom cell is not noticeable in the triple junction structure since the photocurrent of the germanium junction is about twice the photocurrent of GaInP and GaAs [8, 19] and

in the ISO-type cells limited by the simulated top and middle cells. The bandgap of Ge solar cell is substantially low compared to GaInP and GaAs resulting in higher current density J_{sc} , and small degradation after irradiation in the bottom cell is not significant and will not limit the total current. Also, because of lower bandgap, the voltage contribution from Ge will be very less [20]. The excess current density and low

Table 5 J_{sc} of ISO-type and full solar cells

Current density mA/cm ²	Before Radiation test J_{sc} (top)	After Radiation test J_{sc} (top)	Before Radiation test J_{sc} (mid)	After Radiation test J_{sc} (mid)
Full Cell				
Sample 1	17.30	17.27	17.67	17.34
Sample 2	17.05	17.04	17.61	17.6
Sample 3	17.03	16.92	17.63	17.62
Sample 4	17.06	17.05	17.79	17.61
Current density mA/cm ²	Before Radiation test J_{sc}		After Radiation test J_{sc}	
Top Cell				
Sample 1	16.97		16.81	
Sample 2	17.01		16.97	
Sample 3	17.09		17.01	
Sample 4	16.96		16.94	
Middle Cell				
Sample 1	17.8		17.26	
Sample 2	17.65		17.32	
Sample 3	17.28		17.26	
Sample 4	17.63		17.25	
Bottom Cell				
Sample 1	23.95		23.75	
Sample 2	23.99		23.66	
Sample 3	23.94		23.52	
Sample 4	23.98		23.74	

[Sample 1 and 2 are irradiated for 1 MeV electron, 5E14e/cm², 1E14e/cm² fluence, respectively, sample 2 and 3 are irradiated for 10 MeV Proton of 1E12 p/cm², 5E12p/cm², respectively.]

voltage contribution by the Ge bottom cell result in negligible or no effect on the performance of the triple junction cell after irradiation.

In multijunction solar cells, the low current generated top cell (higher bandgap material) limits the total current of the solar cell. Since the degradation of the top cell is less compared to the middle cell, the current performance of the multijunction solar cell is not affected significantly. To achieve this generally GaAs solar cell current density designed to be slightly higher than the top junction, so that, even after radiation exposure the top cell current only will limit the total performance of the solar cell.

4.5 Electroluminescence (EL)

EL measurements give numerous information on materials and device properties. They are therefore widely used for solar cell characterization to assess absorption, resistance losses, or defect levels. They

are fast and non-destructive characterization techniques used across the world.

When a transition from an upper to a lower energy state can occur without emitting a photon, the emission efficiency is decreased. Non-radiative recombination processes are difficult to identify or to study directly because their occurrence can only be inferred from the low emission efficiency [21, 22]. The EL emission reduces after radiation because of defect states and this indicates the non-radiative recombination after radiation [10].

The EL of a solar cell is measured using the current source to control the current injected into the solar cell, the set current is 60 mA (I_{sc} of the solar cell) and the bias voltage is set at 2.6 V (approx. V_{oc} of the solar cell). The light emitted from the cell is directed toward the fiber optic of the spectroradiometer which is connected to a computer. For this purpose, two spectroradiometers were used: a Silicon (Si) based spectroradiometer that detects the ultra-violet and

visible region and an InGaAs-based spectroradiometer that detects the near-infrared region [22, 23].

The band-edge emissions from the respective sub-cells were observed by EL spectroscopy. A typical EL spectrum at room temperature is shown in Fig. 8; the emission around 1.88 eV, 660 nm, and 1.41 eV, 880 nm was observed from the GaInP top cell, the GaAs middle cell, respectively.

The solar cell is examined by EL for non-radiative recombination mechanisms from the top GaInP junction to middle GaAs junction. The magnitude of the non-radiative recombination in the junctions provides a measure of material quality of each junction in the photovoltaic device [8]. EL spectrum of pre- and post-radiation is presented in Fig. 8.

Two peaks are observed in the EL spectrum and indicate the bandgap region of the two top junctions GaInP and GaAs and are shown in Fig. 8. The EL peak intensity of the GaAs cell degraded dramatically after irradiation. This degradation rate was more compared to GaInP the degradation rate of EL intensity of the GaInP cell is much less than that of the GaAs cell, these results confirm that the GaAs cell has low radiation tolerance compared to GaInP [24].

The EL spectrum measured pre and post-electron radiation demonstrates that the non-radiative recombination in the solar cell before radiation is

considerably higher compared to the radiative signal emitted by solar cell after radiation, this indicates that the solar cell after radiation will have defects induced by radiation, due to this the intensity of EL spectrum reduces considerably after irradiation, this information can be used in software simulation to study the defect densities and defects levels after radiation.

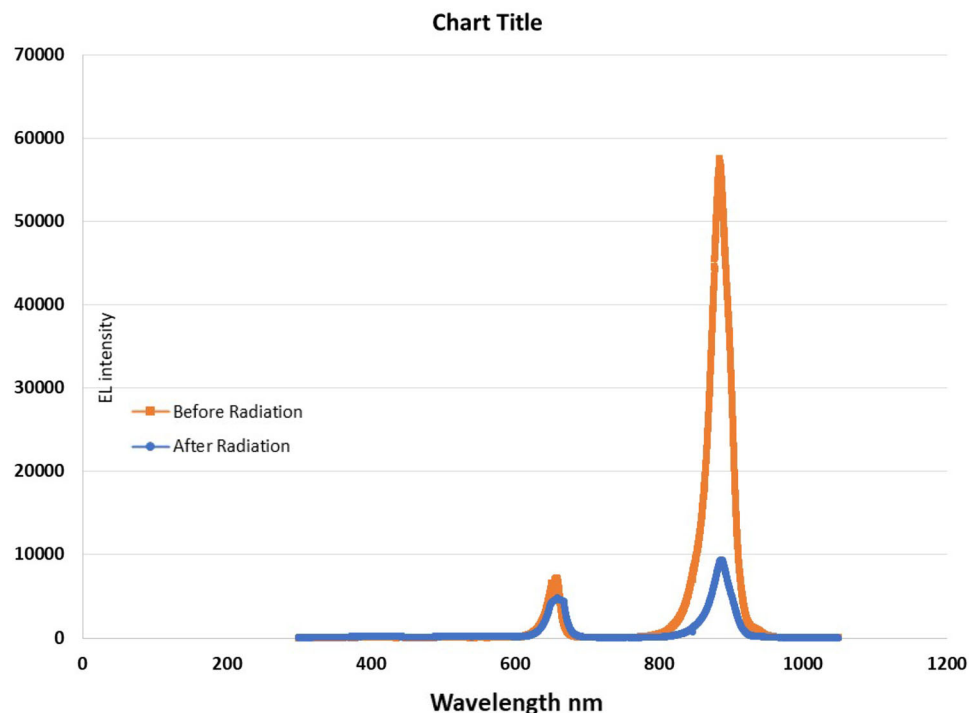
5 Conclusion

Solar cell *I*–*V* measurements, spectral response, and electroluminescence measurements have been used to better understand the mechanism of degradation of solar cell performances.

The saturation current and ideality factors of all sub-cells and full cells are estimated from dark IV characteristics. The results indicates that the ideality factor decreases and saturation current increases with the radiation exposure due to decreased diffusion length and reduced minority carrier lifetime after irradiation. The minority carrier life time decreases with radiation due to introduction of defects which act as recombination centers.

GaAs based multijunction solar cells are more radiation harder than the previous generation single-junction gallium arsenide (GaAs) solar cells. This is due to the higher radiation hardness of the current

Fig. 8 EL of full cell pre & post $5E14 \text{ e/cm}^2$ irradiation



limiting indium gallium phosphide based top cell. Understanding how each sub-cell degrades helps in the design of the multijunction solar cell with improved radiation resistance tolerance. The full and sub-cells/ISO-type cells were irradiated by electron and proton at different fluence level in order to establish the changes. Carried out characterization pre- and post-irradiation to understand the behavior of each sub-cell vis-à-vis the full cell. These studies enable us to understand the degradation behavior of sub-cells of multijunction solar cells and help in the improvement of the solar cell growth process and material selection. These results are used in the modeling of solar cell and helps to model the defect and traps in the solar cells.

Different characterization techniques are used to understand the multijunction solar cell in depth, all the measurements indicate that the GaAs sub-cell is the weakest element of the triple junction structure from a radiation tolerance point of view. The main reason for this is attributable to the introduction of defects in the solar cell due to irradiation resulting in reduced minority carrier lifetime.

This study of sub-cells/ISO-type cells helps in optimization of the solar cell design, material selection and manufacturing processes of multijunction solar cell. Also, these results are useful in modeling of multijunction solar cells and radiation-induced defects in solar cell.

Acknowledgements

This work was supported by U.R. Rao satellite center (URSC). The radiation tests are carried at the Electron Beam Center, and Pelletron, TIFR, Mumbai of Bhabha Atomic Research center (BARC), and the characterization is done at Solar panel division, URSC and Tata Institute of Fundamental Research (TIFR), Mumbai.

Funding

This work was supported by U.R. Rao satellite center (URSC). The radiation tests are carried at the Electron Beam Center, and Pelletron, TIFR, Mumbai of Bhabha Atomic Research center (BARC), and the characterization is done at Solar panel division, URSC and Tata Institute of Fundamental Research (TIFR), Mumbai.

Declarations

Conflict of interest Authors do not have any conflict of interest.

References

1. A. Luque, S. Hegedus, *Handbook of Photovoltaic Science and Engineering*, Wiley, ISBN 0-471-49196-9, (2003)
2. C. Baur, M. Meusel, F. Dimroth, A.W. Bett, M. Neil, G. Strobl, S. Taylor, C. Signorid, *Analysis of the Radiation Hardness of Triple-and Quintuple-Junction Space Solar Cells* (IEEE, Lake Buena Vista, 2005), pp. 548–551
3. B.E. Anspaugh, *GaAs Solar Cell Radiation Handbook* (JPL Publication, NASA, Pasadena, 1996).
4. L. Zhu, M. Yoshita, S. Chen, T. Nakamura, T. Mochizuki, C. Kim, M. Imaizumi, Y. Kanemitsu, H. Akiyama, *IEEE J. Photovolt* **6**(3), 777–781 (2016)
5. H.S. Rauschenbach, *Solar Cell Array Design Handbook* (Van Nostrand Reinhold Co., New York, 1980).
6. S.M. Sze, *Semiconductor Devices*, Wiley, Second Edition, ISBN 0-471-33372-7 (Wiley, 2003)
7. E.L. Meyer, *Int. J. Photoenergy* **8479487**, 9 (2017)
8. H. Sugimoto, M. Tajima, S. Hasel, M. Imaizumi, *Luminescence Analysis of Radiation Effects in Multijunction Solar Cells for Space* (IEEE, Lake Buena Vista, 2005), pp. 830–833
9. D. Walker, J. Nocerino, Y. Yue, C.J. Mann, S.H. Liu, *Subcell Light Current–Voltage Characterization of Irradiated Multijunction Solar Cell* (IEEE, Washington, DC, 2015), pp. 93–95
10. Y. Yana, M. Fangc, X. Tanga, F. Chena, H. Huanga, X. Suna, L. Jia, *Nucl. Instrum. Methods Phys. Res. B* **451**, 49–54 (2019)
11. A.M. Humada, M. Hojabri, S. Mekhilef, H.M. Hamada, *Renew. Sustain. Energy Rev.* **56**, 494–509 (2016)
12. F. Ghani, M. Duke (IEEE Photovoltaic Specialist Conference, 2011), pp. 2861–2865
13. S. Banerjee, Electron irradiation effects on the shunt resistance of silicon solar cells. *Solar Cells* **20**, 315–321 (1987)
14. T. Nakamura, M. Imaizumi, M. Sugai, S.-I. Sato, T. Ohshima. JAXA Special Publication JAXA-SP-12-008E, pp 50–53
15. T. Nakamura, M. Imaizumi, S.-I. Sato, T. Ohshima (IEEE Photovoltaic Specialist Conference, 2011), pp. 2846–2850
16. S. Michael, RADECS proceedings (2005)
17. A.L. Crespín, S. Michael, 22nd AIAA International Communications Satellite Systems Conference (2004)
18. V. Paraskeva, M. Hadjipanayi, M. Norton, M. Pravettoni, G.E. Georgiou (IEEE, 2014), pp. 3664–3669

19. H.L. Cotal, R.R. King, M. Haddad, J.H. Ermer, N.H. Karam, D.D. Krut, D.E. Josh, M. Takahashi, B.T. Cavicchi, *The Effects of Electron Irradiation on Triple-Junction Ga/Sub 0.5/In/Sub 0.5/P/GaAs/Ge Solar Cells* (IEEE, Piscataway, 2000), pp. 1316–1319
20. Y. Sheng-sheng, G. Xin, F. Zhan-zu, Z. Lei, C. Xin-yu, Proc. RADECS 2013 and IEEE (2013), PI(2), pp 1–5
21. R. Hoheisel, F. Dimroth, A.W. Bett, S.R. Messenger, P.P. Jenkins, R.J. Walters, *Solar Energy Mater. Solar Cells* **108**, 235–240 (2013)
22. J.I. Pankove, *Electroluminescence* (Springer, Berlin, Heidelberg, New York, 1977).
23. A. Gauffier, J.P. David, O. Gilard, T. Nuns, C. Inguibert, A. Balocchi, *IEEE Trans. Nucl. Sci.* **56**(4), 2237–2241 (2009)
24. S. Roensch, R. Hoheisel, F. Dimroth, A.W. Bett, *Appl. Phys. Lett.* **98**, 251113 (2011)
25. C. Baur, A.W. Bett *IEEE Photovoltaic Specialist Conference* (2010), pp. 1100–1105

Publisher's Note Springer Nature remains neutral with regard to jurisdictional claims in published maps and institutional affiliations.